ADVANCED FUNCTIONAL MATERIALS
www.afm-journal.de

Flexible and Controllable Piezo-Phototronic Pressure Mapping Sensor Matrix by ZnO NW/p-Polymer LED Array

Rongrong Bao, Chunfeng Wang, Lin Dong, Ruomeng Yu, Kun Zhao, Zhong Lin Wang,* and Caofeng Pan**

A functional tactile sensing device is essential for next-generation robotics and human–machine interfaces technologies, since the emulation of touching requires large-scale pressure sensor arrays with distinguishable spatial-resolution, high sensitivity, and fast response. Here, a flexible LED array composed of PEDOT:PSS and patterned ZnO NWs with a spatial resolution of 7 μm for mapping of spatial pressure distributions is designed and fabricated. The emission intensity of the LED array sensor matrix is dominated by locally applied strains as indicated by the piezo-phototronic effect. Therefore, spatial pressure distributions are immediately obtained by parallel-reading the illumination intensities of the LED arrays based on an electroluminescence working mechanism. A wide range of pressure measurements from 40 to 100 MPa are achieved through controlling the growth conditions of the ZnO nanowire array. These devices may find prospective applications as electronic skins by taking advantage of their high spatial-resolution, flexibility, and wide pressure mapping range.

1. Introduction

A functional tactile sensing device is mandatory for next-generation robotics and human–machine interfaces since the emulation of touching requires large-scale pressure sensor arrays with high-spatial resolution, high sensitivity, and fast response.[1] Some tactile sensors fabricated with organic transistors or microstructured rubber layer pressure sensor arrays have been reported,[2] whose working mechanism is based on changes in capacitance or resistance. While with a resolution at the order of millimeter, these devices have not yet met the requirements of artificial skins whose spatial resolution is near 50 μm. Our group has demonstrated pressure sensor array base on piezotronic[3] and piezo-phototronic effects.[4] A spatial resolution of 120 μm was achieved for piezotronic pressure sensor array,[5] and an ultrahigh resolution of 2.7 μm was derived from a piezophototronic pressure sensor array using a ZnO nanowire (NW)/p-GaN LEDs array.[6] These devices provide stable, fast-response, and parallel-reading detections of spatial pressure distributions. However, the lacking of flexibility with a rigid sapphire substrate prevents the NW-LEDs array device from applications as smart skin, and the pressure measuring range of the device is in a relatively high-pressure region. Therefore, a flexible pressure mapping system with moderate spatial resolution becomes necessary and may find numerous potential applications in human–machine interfaces.

Organic/inorganic hybridized LEDs draw tremendous attentions because of their high flexibility. Among them, n-ZnO and p-poly(3,4-ethylenedioxythiophene)-polystyrenesulfonate (PEDOT:PSS) hybridized inorganic/organic LED has aroused great technological and scientific interests due to the excellent optoelectronic properties of ZnO and the high flexibility, low-cost, easy fabrication, potential for large area deposition and commercial availability of PEDOT:PSS.[7] Here, we demonstrate a flexible LED array composed of PEDOT:PSS and patterned ZnO NWs for mapping spatial pressure distributions. By utilizing strain-induced negative piezoelectric polarization charges presented at the local interface of the p–n junction, the piezo-phototronic effect has been applied to modify the band structure through reducing the barrier height for hole injections from the PEDOT:PSS side, and thus facilitate the recombination between electrons and holes in the ZnO side for enhancement of light-emitting intensity. Therefore, the pressure distribution is obtained by parallel-reading the illumination intensities of the LED pressure sensor array. The spatial resolution as high as 7 μm is achieved by fabricating ZnO nanowires on a flexible substrate. By controlling the growth conditions of the ZnO NW array, a wide range of pressure measurements from 40 to 100 MPa are derived under different ZnO morphologies. These devices may find prospective applications as electronic skins by taking advantage of their high spatial-resolution, flexibility, and wide pressure mapping range.

Dr. R. Bao, C. Wang, Prof. L. Dong, K. Zhao, Prof. Z. L. Wang, Prof. C. F. Pan
Beijing Institute of Nanoenergy and Nanosystems
Chinese Academy of Sciences
Beijing, P.R. China
E-mail: ldong@zzu.edu.cn; zhong.wang@mse.gatech.edu; cfpan@binn.cas.cn
C. Wang, Prof. L. Dong
School of Materials Science and Engineering
Zhengzhou University
Zhengzhou 450001, P.R. China
R. Yu, Prof. Z. L. Wang
School of Materials Science and Engineering
Georgia Institute of Technology
Atlanta, GA 30332-0245, USA

DOI: 10.1002/adfm.201500801

2. Result

Hexagonal structured wurtzite crystals possess an obvious anisotropic property along and perpendicular to the c-axis direction. For noncentral symmetric crystals, such as ZnO and GaN, piezoelectric property is naturally observed once the material is strained. Simply speaking, the centers of Zn^{2+} cations and O^{2-} anions are tetrahedrally coordinated and overlapped with each other at initial state, upon straining, the relative displacement of centers of the cations and anions leads to a dipole moment, which is the piezoelectric potential (piezo-potential). In a p–n-junction LED, associated with this piezo-potential, piezoelectric polarization charges are hence induced in the vicinity of the local interface to modify the energy band structures and thus tune/control the optoelectronic process, such as generation, separation, recombination, and/or transport of charge carriers. This is known as the piezo-phototronic effect. Mapping of spatial pressure distributions is, therefore, achieved by the piezo-phototronic effect since the light-emitting intensity of individual NW-LEDs depends on the local pressure exerted on it. A schematic illustration of the flexible NW-LED-based pressure sensor array after applying a compressive strain is shown in **Figure 1**.

Figure 1. Schematic illustration of the flexible NW-LED-based pressure sensor array after applying a compressive strain. The device is based on a ZnO NW/p-polymer array. The inset is a photograph of the flexible device.

The device was fabricated based on a patterned array of n-ZnO NWs synthesized on an ITO/PET substrate, with the c-axis pointing upward. After infiltrating the inter-nanowire space with SU8 and spin-coating a layer of PEDOT:PSS, an Au film was deposited on the top of the PEDOT:PSS to form a common electrode. The fabrication process is schematically illustrated in **Figure 2**a, using a transparent ITO/PET substrate as a negative electrode for electron injection and an Au metal contact as a positive electrode for hole injection. Figure 2b–d shows the SEM images of the as-grown ZnO NWs. Patterned arrays of the ZnO nanowires with a diameter of 300 nm and length of 4 μm were synthesized above the ZnO seed layer,

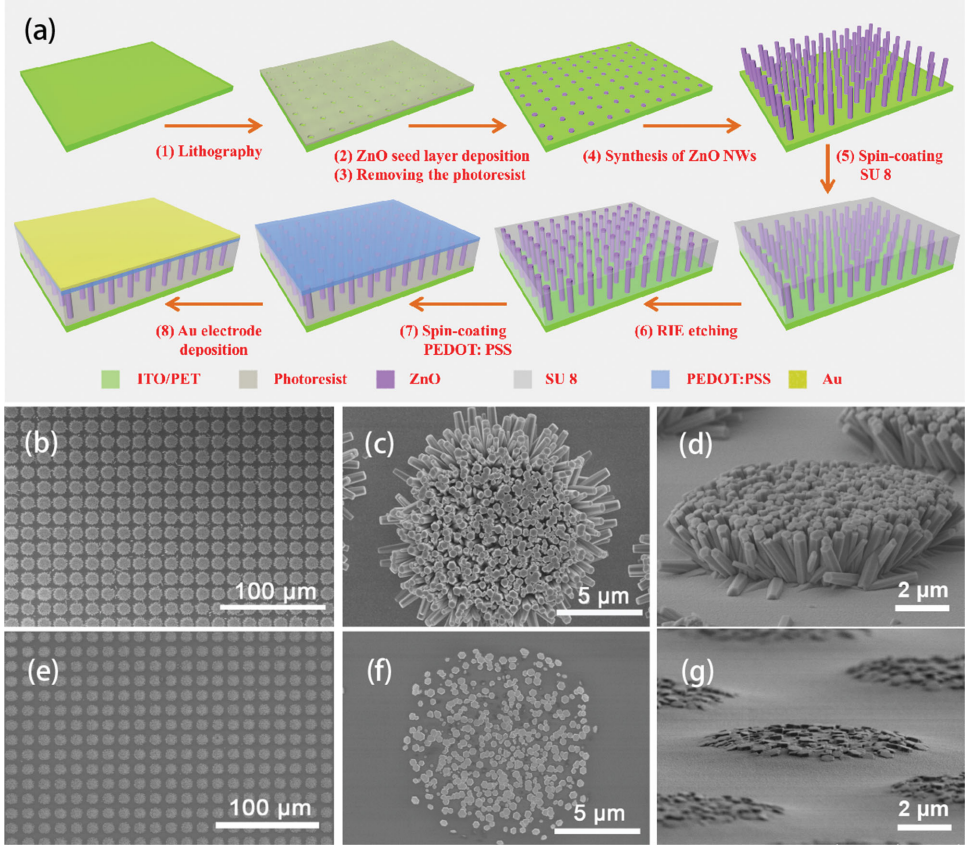

Figure 2. a) Schematic illustration of the fabrication process of a ZnO NW/p-polymer LEDs array. b–d) SEM images of the as-grown ZnO NWs. e–g) SEM images of the as-grown ZnO NWs immersed in SU8 with their tips exposed.

Adv. Funct. Mater. **2015**,
DOI: 10.1002/adfm.201500801

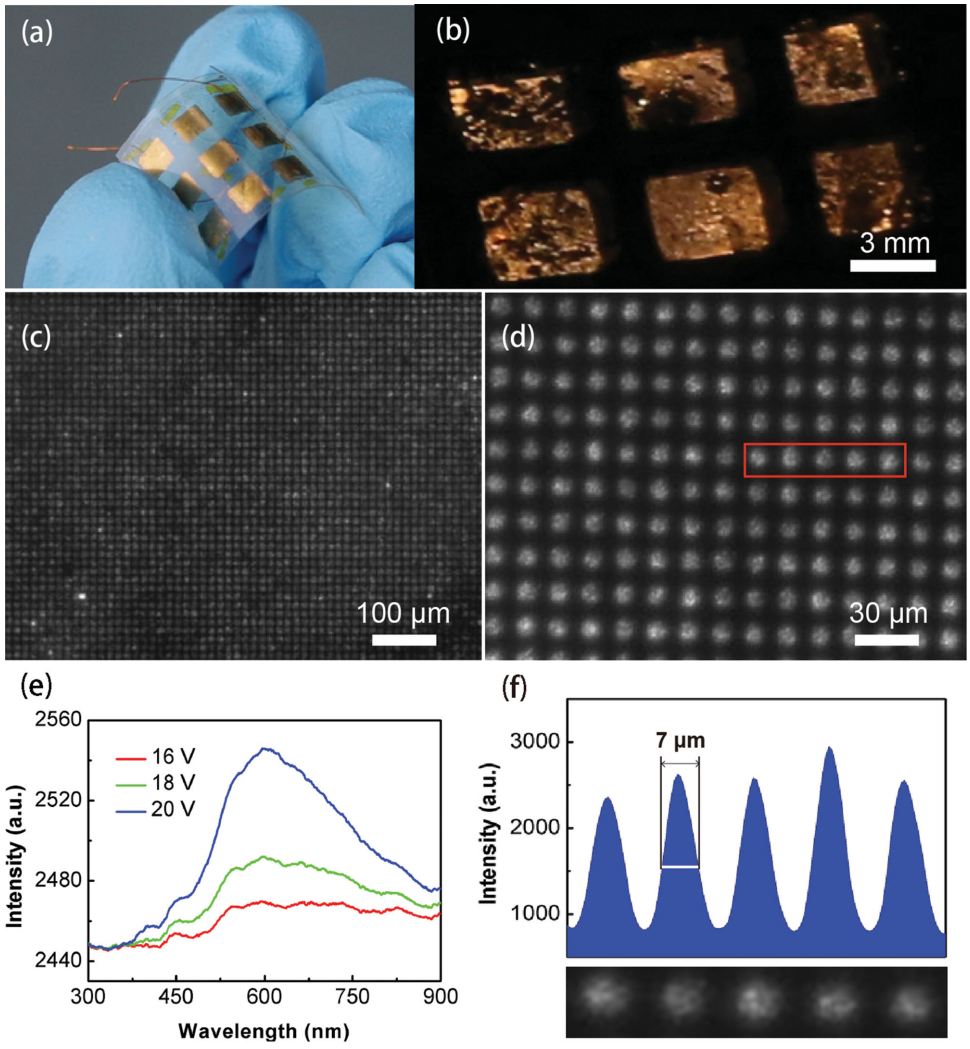

Figure 3. a,b) Optical images of a fabricated flexible device and the corresponding image when the device was electrically lit up, showing yellow–white light emission from the NW-LED array. c,d) Optical images of a ZnO NW/p-polymer LEDs array device. e) Room temperature EL spectra of the ZnO NW/p-polymer LED under different biased voltages. f) Five typical nanowire LEDs (marked with a red rectangle in (d)) and the corresponding line profile of their emission intensity.

with a side length of 5 μm and a pitch of 15 μm (Figure 2b). A layer of SU8 was spun coated to immerse the ZnO NWs afterward, followed by oxygen plasma etching of SU8 to expose the heads of the ZnO NWs. Figure 2e–g and S1 clearly shows the exposures of ZnO NWs tips after oxygen plasma etching, with the bottoms and main bodies of the NW arrays being fully enclosed, which greatly improves the stability and robustness of the structure. Finally, a layer of PEDOT:PSS was spun coated on the top of the ZnO NWs, and a 40 nm layer of Au was then sputtered as the top electrode of the device.

The corresponding optical images of a flexible pressure mapping device are presented in **Figure 3**a,b. The electroluminescence performances of the ZnO NWs/p-polymer LEDs array derived under a bias voltage of 18 V are shown in Figure 3c,d. An enlarged image of five adjacent representative LEDs (marked with a red solid rectangle in Figure 3d) is presented in Figure 3f, together with the corresponding line profile of their emission intensity, from which no crosstalk between adjacent light-emitting pixels is observed. Room temperature electroluminescence (EL) spectra of an LED under different bias voltages are shown in Figure 3e. A broad defect-related visible emission ranging from 450 to 780 nm, as well as a weak near band emission (NBE) peak at 400 nm, is observed, which are associated with the nonperfect crystallinity and high defect concentrations of ZnO NW synthesized through the low-temperature hydrothermal method[8] (PL spectra of ZnO NWs are shown in Figure S2, Supporting Information). EL intensity increases as the voltage increases, whereas the peak does not show any obvious shift. The mapping resolution is near 7 μm, as defined by the full-width at half-maximum (FWHM) of the emission pixels.

To determine the impact of piezo-phototronic effect on the device light emission performance, pressure mapping performances of ZnO NWs/p-polymer LED array devices are investigated by pressing a stamp (shaped in "BINN") made of SU8 on the device as shown in **Figure 4**. Obvious light emissions are

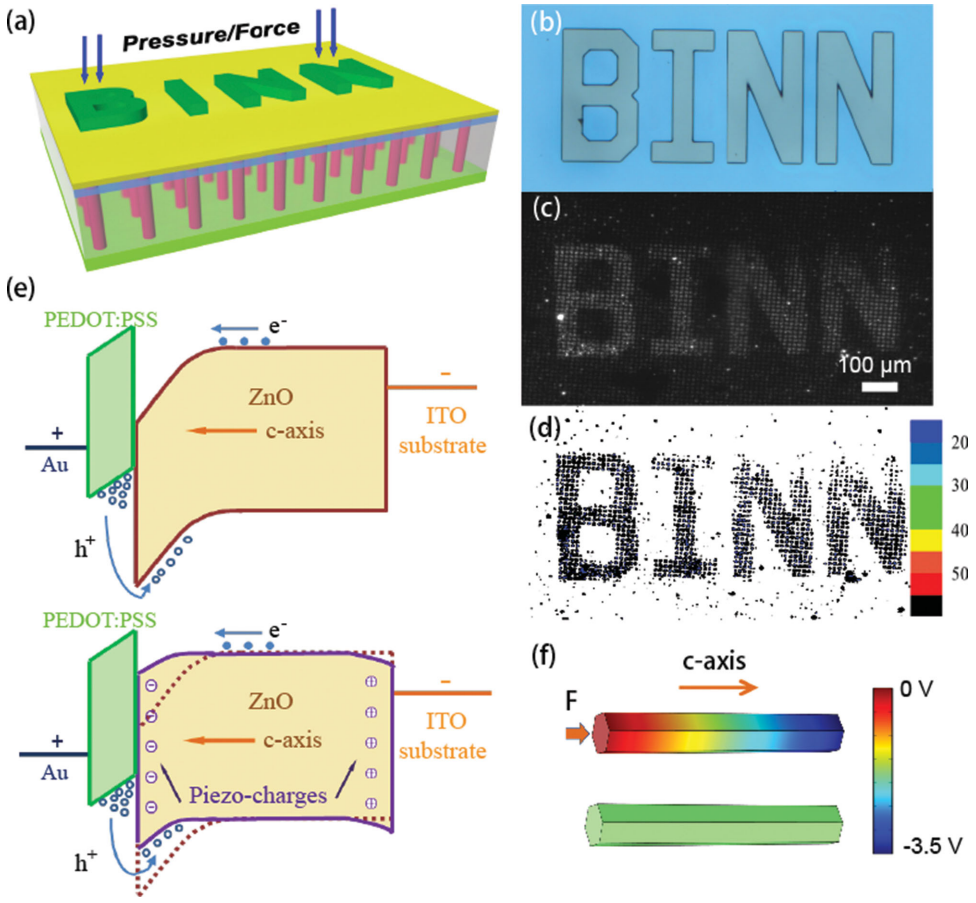

Figure 4. a) Schematic illustration of the NW-LED-based pressure sensor array for imaging pressure distribution. b) Optical image of the convex-character pattern of "BINN." c) Electroluminescence image of the device at a stress of 80 MPa. The image clearly shows that a change in LED intensity occurred at the pixels that were compressed, whereas those away from the pattern on mask showed almost no change. d) 2D contour map of the factor derived from the LED intensity images. It directly presents the word "BINN," as given on the convex-character pattern substrate. e) Schematic band diagram of an n-ZnO/p-polymer p–n junction before (top) and after (solid line in the bottom) applying a compressive strain; the local negative piezoelectric charges at the p–n junction region will raise the energy band in the ZnO nanowire near the junction region. f) Piezo-potential distributions in a ZnO nanowire under a pressure of 200 MPa simulated by a finite-element analysis method (COMSOL). The diameter and length used for the calculation are 400 nm and 3 μm, respectively. The conductivity of the ZnO nanowire is ignored in the simulation for simplicity.

observed from NW LEDs under pressure (Figure 4b,c) due to the piezo-phototronic effect that effectively modulates the light emission intensity through applied strains. Detailed experimental setup with the measurement system has been provided in Supporting Information (Figure S3). The NW-LED array can be uniformly lit up under a bias of 16 V. The electroluminescence image of the device at a stress of 80 MPa is shown in Figure 4c. The image clearly shows that a change in LED intensity occurred at the pixels that were compressed, whereas those away from the pattern on the mask showed almost no change. Figure 4d shows a 2D contour map of the factor derived from the LED intensity image shown in Figure 4c. It directly presents the word "BINN," as given on the convex-character pattern substrate.

Figure 4e shows the energy band diagram of the ZnO NW/p-polymer LED. There is a 0.9 eV barrier for electron injection from the conduction band of ZnO into LUMO of PEDOT:PSS. The hole injection barrier is approximately 2.4 eV for hole transfer from HOMO of PEDOT:PSS into valence band of ZnO.[9] The electron and hole accumulation at the ZnO/PEDOT:PSS interface will be substantial under a forward bias, leading to a light emission by electron–hole recombination.[10] Straining the basic unit cell of ZnO results in the polarization of the cations and anions in the crystal because of its non-central symmetric structure, which induces the inner-crystal piezo-potential. An important factor influencing the conversion efficiency of LED is the current balance and carrier mobility of electrons and holes. According to the room-temperature EL spectra of the ZnO NW/p-polymer LED, the light emission occurs only in the ZnO NW. In our device, electrons are the majority carriers,[11] and recombination is limited by the hole injection rate due to the large barrier height (2.4 eV) and low mobility for hole transport.[12] When the ZnO NWs are under compressive strains, a negative piezo-potential is produced at the local interface of the ZnO/p-polymer p–n junction. The corresponding negative piezoelectric polarization charges thus raise the energy band in the ZnO side in the vicinity of the junction region, leading to a reduced barrier height for hole

DOI: 10.1002/adfm.201500801

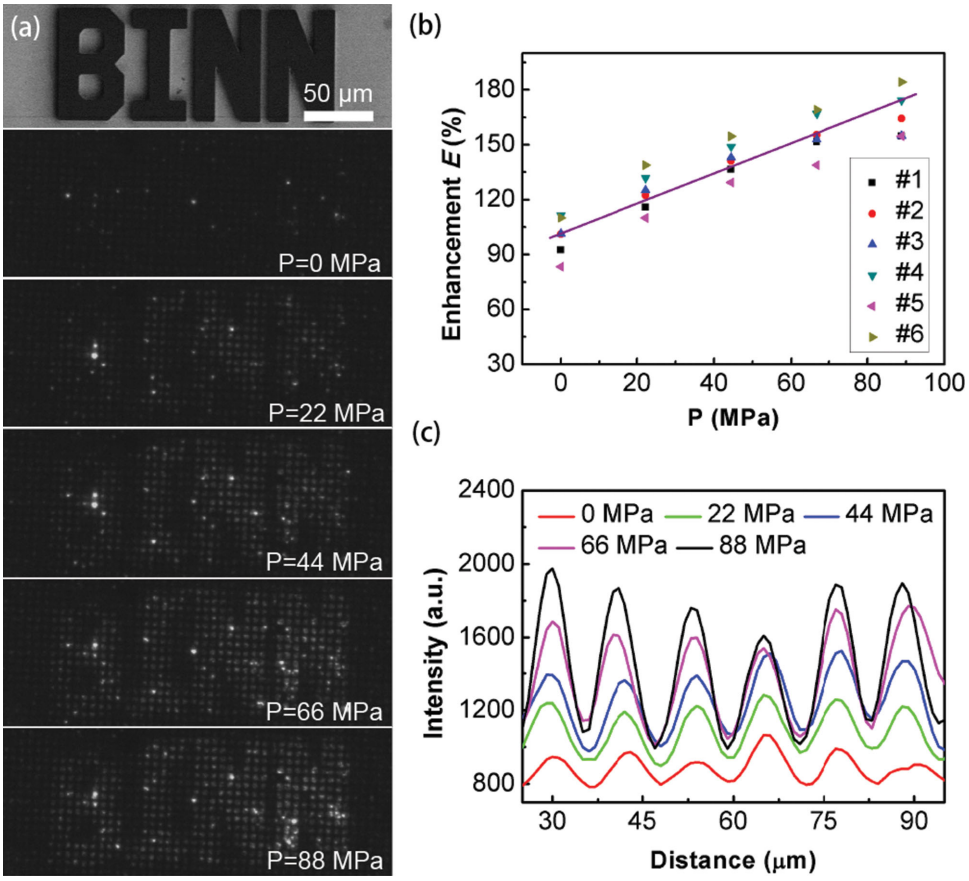

Figure 5. a) Optical images of the convex-character pattern of "BINN" and electroluminescence images of the device at pressure of 0, 22, 44, 66, and 88 MPa, respectively. These images clearly show that a change in LED intensity occurred at the pixels that were compressed, whereas those away from the convex-character pattern showed almost no change. b) Enhancement factor E of six NW-LEDs as a function of an applied compressive pressure of up to 88 MPa. c) The line profile data of the signal-to-noise ratio derived under different pressures.

injection. Therefore, the modified band structure increases the hole injection rate from PEDOT:PSS into ZnO and the recombination rate of electrons and holes in the ZnO NWs, leading to an enhancement of the light emission intensity. Figure 4f shows the simulated piezo-potential distributions in a ZnO NW under a pressure of 200 MPa by a finite-element analysis method (COMSOL). The diameter and length used for calculation are 400 nm and 3 μm, respectively. The conductivity of the ZnO NW is ignored in the simulation for simplicity. The simulation presented here may help us for a better understanding of the core physics of the piezo-phototronic devices.

The intensities of light emissions of the device were systematically studied under different pressures of 0, 22, 44, 66, and 88 MPa, as shown in **Figure 5**a. The images clearly show that the stronger the pressure was applied, the stronger the light intensity was derived. And the changes in LED illumination intensity only occurred at pixels that were compressed by the stamp. The enhancement factor E of the LED intensity is defined as $E = I_p/I_0$, where I_0 and I_p are the intensities of the LED under zero and corresponding pressures, respectively. Figure 5b shows a linear dependence of the enhancement factor E on the pressure. The signal-to-noise ratio of the E factor obtained from six adjacent NW-LEDs under different pressures is presented in Figure 5c, clearly indicating a higher illumination intensity under a stronger pressure.

The sensor sensitivity S[4,13] in terms of relative light intensity enhancement as a function of applied pressure is defined as

$$S = \frac{\Delta I / I_0}{\sigma} = \frac{(E-1)}{\sigma} \quad (1)$$

where E is the enhancement factor, $\Delta I = I_p - I_0$, and σ is the pressure applied to each ZnO NW. Considering the construction of these devices that each pixel is composed of numerous ZnO NWs, the pressure applied on NWs is determined by

$$\sigma = \frac{P}{\Delta a / a} \quad (2)$$

P is the pressure applied to the whole device, a is the total area of the pixel (i.e., a square), whereas Δa is the area of ZnO NWs with the head exposed in each pixel. Therefore, under the same external pressures, the actual strains applied on ZnO NWs differ from one another for devices with different NWs geometries, indicating the possibility to tune/control light intensity enhancement of the array device by varying the density and diameter of the ZnO NWs in each pixel. Different concentrations of nutrient solution (from 40 to 80 × 10^{-3} M) were

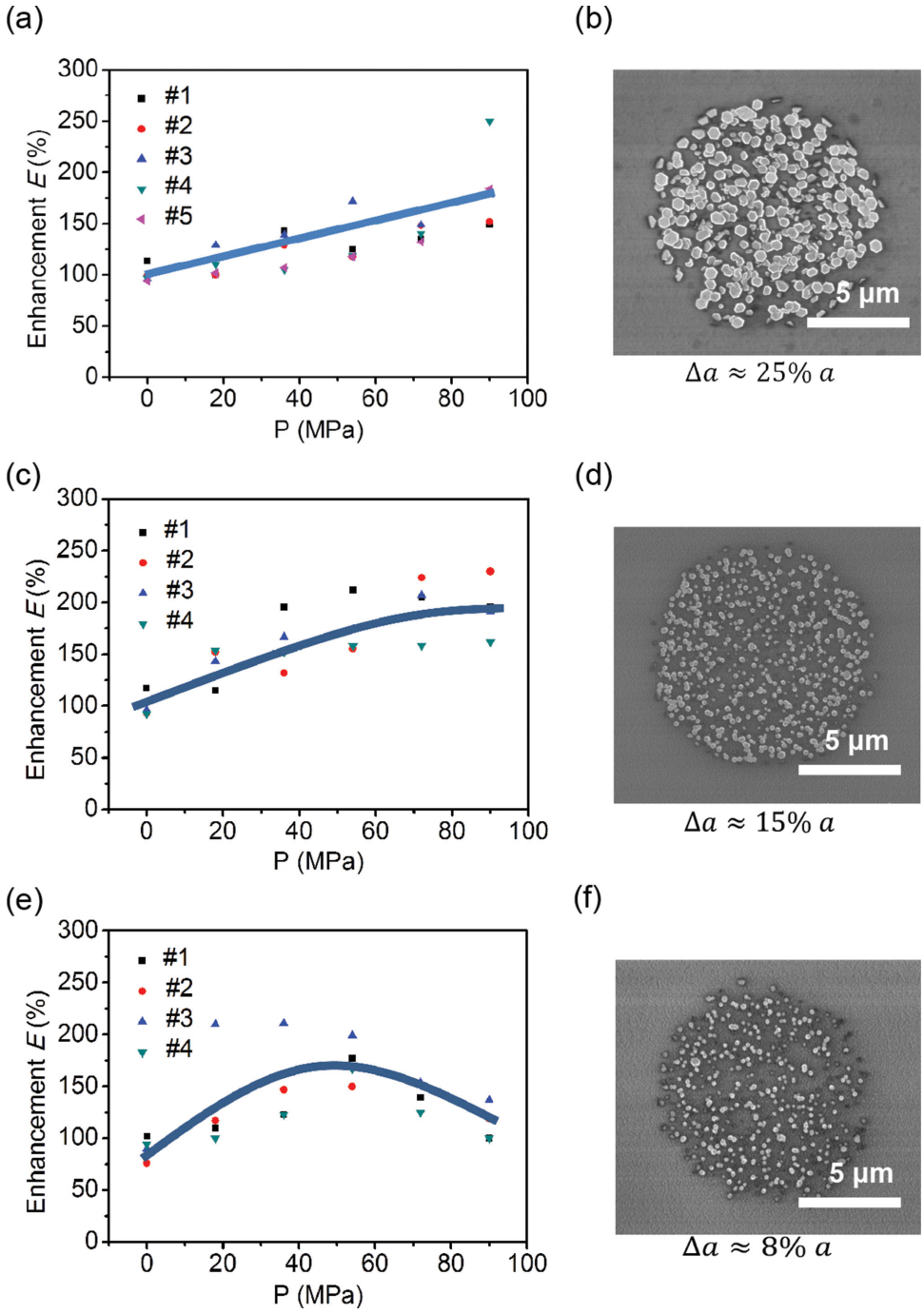

Figure 6. Light intensity enhancement of device with different NW geometries under the same external pressures. a,c,e) Enhancement factor E of an NW-LED as a function of the applied pressures with the ZnO NWs synthesized in a) 80×10^{-3} M, c) 60×10^{-3} M, and e) 40×10^{-3} M nutrient solutions. b,d,f) The corresponding SEM images of ZnO NWs synthesized in b) 80×10^{-3} M ($\Delta a \approx 25\% a$), d) 60×10^{-3} M ($\Delta a \approx 15\% a$), and f) 40×10^{-3} M ($\Delta a \approx 8\% a$) nutrient solutions.

employed for ZnO NWs synthesizing to derive various geometries of the nanostructure, leading to controllable length, diameter, and density of ZnO NWs as shown in **Figure 6** and Figure S4 (Supporting Information). The light intensity enhancement factor E of devices with every NWs geometry is carefully investigated by applying a series of pressures externally and summarized in Figure 6. The ZnO NWs array device synthesized in high concentration (80×10^{-3} M) of nutrient solution possesses larger area of exposed ZnO tips Δa and thus lower E, as shown in Figure 6a. Meanwhile, a nonlinear increase of E with externally applied pressures is derived for a device fabricated in a 60×10^{-3} M nutrient solution (Figure 6c) reaching a saturation point at 70 MPa pressure. In Figure 6e, a maximum enhancement factor E is observed near 50 MPa

Adv. Funct. Mater. **2015**,
DOI: 10.1002/adfm.201500801

pressure because the pressure exceeding 50 MPa will cause damages to the device. As shown in Figure S5 in Supporting Information, the current and the LED intensity increase when the pressure was loaded, and then the LED is broken down and its current increases suddenly, becoming a short circuit behavior, when the pressure is increased beyond the maximum range of that the device can withstand. The maximum stress we applied on the device (Figure 6) is about 100 MPa, which is only about 1% of the breaking strength of ZnO NW, which is reported to be about 3–13 GPa.[14] So, we found that the short circuit failure of the LED is caused by the break of the PEDOT:PSS layer, not the break of ZnO NWs. Therefore, according to the actual application requirement, the pressure measurement range of the LED mapping system can be controlled varying from 40 to 100 MPa by changing the growth conditions of the ZnO NWs array. The flexibility and stability of the LED array mapping system are studied and presented in Figure S6 (Supporting Information). No significant fluctuations of the sensing performances were observed after repetitively bending and releasing the device for over 300 cycles.

3. Discussion

Such a piezoelectric organic/inorganic hybrid Nano-LED-based approach offers a few unique advantages for imaging strain distribution and may have potential applications for e-skin and human–machine interfacing. First, the current device is truly flexible by introducing the p-polymer instead of the GaN/sapphire hard substrate that we used in the previous work. This makes the device more like a "skin." Second, the spatial resolution of the device could be further improved. In general, the spatial resolution depends on lithography (LED size), illumination detection (sensitivity), and so on. In this experiment, we used the patterned pore with a diameter of about 5 μm, which was prepared by photolithography (PL). According to Rayleigh criteria and our previous study,[6] the estimated resolution R for our devices is R (μm) = D + 1.2 (μm), where D (μm) is the diameter of the NWs. If the diameter of the ZnO can be reduced to 100 nm with e-beam lithography, we could obtain a resolution of 1.3 μm. Considering the cost, we choose 7 μm as the resolution of the current device, which is much better than the resolution of human skin (50 μm). Third, it should be noted that the response time of the device is mostly due to the slower period of time for applying/retracting a mechanical force, which takes a longer time than the physics of the device itself (e.g. hole-injection rate), illumination detection rate, and other electronics. This means that the response time is fast for the potential tactile sensing application.

4. Conclusions

In summary, we designed and fabricated a flexible LED array composed of PEDOT:PSS and patterned ZnO NWs with a spatial resolution of 7 μm for mapping of spatial pressure distributions. By using the piezo-phototronic effect, strain-induced polarization charges presented in the vicinity of local interface effectively modify the band structure through reducing the barrier height for hole injections from the PEDOT:PSS side, and thus facilitate the recombination between electrons and holes in the ZnO side for enhancing light-emitting intensity. Therefore, pressure distribution is obtained by parallel-reading the illumination intensities of LED arrays based on an electroluminescence working mechanism. These devices possess a wide range of pressure measurements from 40 to 100 MPa depending on the growth conditions of ZnO NWs. The outstanding flexibility, high resolution, and controllability of these pressure-mapping sensors provide promising technologies for future applications in biological sciences, human–machine interfacing, smart sensor and processor systems, and even defense technology.[15]

5. Experimental Section

Fabrication of the Device: The PET substrates were cleaned ultrasonically in acetone, isopropyl alcohol, and deionized water for 10 min, respectively, and then blown dry with nitrogen gas. An SU8 (from MICROCHEM) photoresist layer, with a patterned pore diameter of about 5 μm and 15 μm pitch, was prepared by photolithography (PL). Subsequently, a 50 nm thickness ZnO seed layer was deposited onto the as-fabricated substrate by RF magnetron sputtering. By removing the photoresist, a substrate with a patterned ZnO seed layer was obtained. Then, the patterned substrate was put into the nutrient solution, containing 50×10^{-3} M zinc nitrate and equal concentration of hexamethylenetetramine (HMTA) for ZnO growth at 85 °C for 3 h. After the growth of patterned ZnO NWs, a layer of SU8 was spun coated wrap around the ZnO NWs. Then, an oxygen plasma etching was applied to etch away the top part of the SU8 and expose the heads of ZnO NWs. At last, a layer of PEDOT:PSS was spun coated on the top of the ZnO NWs and a 40 nm layer of Au was then sputtered as the top electrode of the device.

Characterization: A field-emission scanning electron microscope (FE-SEM, Hitachi SU8020) was used to characterize the morphology of ZnO NWs. The optical images and lighted-up image of the LEDs array were obtained by a Zeiss Observer Z1 inverted microscope equipped with an HQ2 camera. Electroluminescence spectra (EL) were collected by an Ocean Optics QE65000 Spectrometer. The measurement system was built based on an inverted microscope (Zeiss Observer Z1) at 3D micromanipulation stages. A normal pressure was applied on the NW-LEDs using a sapphire substrate with a convex character pattern of "BINN" on it. By controlling the 3D micromanipulation stages and the positioning stage, the pressure could be applied step by step with a fixed amount. The output light intensity was recorded by an HQ2 camera. We mainly focused on the relative change in output light intensity under different pressures. We monitored the pressure change from the change in light-emitting intensity using image acquisition and processing technologies.

In the bending test, the LED device (with a length of 2 cm, a width of 1.5 cm, and a thickness of 0.125 mm) was attached on a PS substrate (with a typical length of 5 cm, a width of 3 cm, and a thickness of 0.5 mm). A linear motor was used for applying a programmed repeated driving strain. When the substrate was bent, the LED device was also bent subsequently with a bending radius of about 2.4 cm. After certain cycles of bending, we lit up the LED and measured the corresponding light intensity, and then continued bending.

Supporting Information

Supporting Information is available from the Wiley Online Library or from the author.

Acknowledgements

R.B. and C.W. contributed equally to this work. The authors thank for the support from the "thousands talents" program for pioneer researcher and his innovation team, China; President Funding of the Chinese Academy of Sciences, National Natural Science Foundation of China (Nos. 51272238, 21321062, 51432005, and 61405040), the Innovation Talent Project of Henan Province (No. 13HASTIT020), Talent Project of Zhengzhou Univ (ZDGD13001), and Surface Engineering Key Lab of LIPCAST.

Received: February 28, 2015
Published online:

[1] a) S. C. B. Mannsfeld, B. C. K. Tee, R. M. Stoltenberg, C. V. H. H. Chen, S. Barman, B. V. O. Muir, A. N. Sokolov, C. Reese, Z. Bao, *Nat. Mater.* **2010**, *9*, 859; b) J. J. Boland, *Nat. Mater.* **2010**, *9*, 790; c) K. Takei, T. Takahashi, J. C. Ho, H. Ko, A. G. Gillies, P. W. Leu, R. S. Fearing, A. Javey, *Nat. Mater.* **2010**, *9*, 821.

[2] a) B. C. K. Tee, A. Chortos, R. R. Dunn, G. Schwartz, E. Eason, Z. A. Bao, *Advanced Functional Mater.* **2014**, *24*, 5427; b) Y. Wang, L. Wang, T. T. Yang, X. Li, X. B. Zang, M. Zhu, K. L. Wang, D. H. Wu, H. W. Zhu, *Advanced Functional Mater.* **2014**, *24*, 4666; c) C. Y. Hou, H. Z. Wang, Q. H. Zhang, Y. G. Li, M. F. Zhu, *Advanced Mater.* **2014**, *26*, 5018; d) S. Jung, J. H. Kim, J. Kim, S. Choi, J. Lee, I. Park, T. Hyeon, D. H. Kim, *Advanced Mater.* **2014**, *26*, 4825; e) Q. Sun, D. H. Kim, S. S. Park, N. Y. Lee, Y. Zhang, J. H. Lee, K. Cho, J. H. Cho, *Advanced Mater.* **2014**, *26*, 4735.

[3] a) Z. L. Wang, J. H. Song, *Science* **2006**, *312*, 242; b) Z. L. Wang, R. S. Yang, J. Zhou, Y. Qin, C. Xu, Y. F. Hu, S. Xu, *Mater. Sci. Eng. R-Rep.* **2010**, *70*, 320.

[4] a) Z. L. Wang, *Nano Today* **2010**, *5*, 540; b) Z. L. Wang, *Advanced Mater.* **2012**, *24*, 4632.

[5] W. Z. Wu, X. N. Wen, Z. L. Wang, *Science* **2013**, *340*, 952.

[6] C. F. Pan, L. Dong, G. Zhu, S. M. Niu, R. M. Yu, Q. Yang, Y. Liu, Z. L. Wang, *Nat. Photonics* **2013**, *7*, 752.

[7] a) B. K. Sharma, N. Khare, S. Ahmad, *Solid State Commun.* **2009**, *149*, 771; b) D.-H. Lee, D.-H. Park, S. Kim, S. Y. Lee, *Thin Solid Films* **2011**, *519*, 5658; c) Q. Yang, Y. Liu, C. Pan, J. Chen, X. Wen, Z. L. Wang, *Nano Lett.* **2013**, *13*, 607.

[8] Z. Wang, J. Qi, X. Yan, Q. Zhang, Q. Wang, S. Lu, P. Lin, Q. Liao, Z. Zhang, Y. Zhang, *RSC Adv.* **2013**, *3*, 17011.

[9] M. Riaz, J. Song, O. Nur, Z. L. Wang, M. Willander, *Adv. Functional Mater.* **2011**, *21*, 628.

[10] a) H. Liu, R. Peng, S. Chu, S. Chu, *Appl. Phys. Lett.* **2014**, *105*, 043507; b) J. Goldberger, D. J. Sirbuly, M. Law, P. Yang, *J. Phy. Chem. B* **2004**, *109*, 9.

[11] S.-H. Yang, Y.-J. Lin, H.-C. Chang, Y.-H. Chen, *Thin Solid Films* **2013**, *545*, 476.

[12] Q. Wei, M. Mukaida, Y. Naitoh, T. Ishida, *Advanced Mater.* **2013**, *25*, 2831.

[13] Y. Gao, Z. L. Wang, *Nano Lett.* **2007**, *7*, 2499.

[14] Mo-R. He, J. Zhu, *Phy. Rev. B* **2011**, *83*, 161302

[15] a) F. Patolsky, B. P. Timko, G. H. Yu, Y. Fang, A. B. Greytak, G. F. Zheng, C. M. Lieber, *Science* **2006**, *313*, 1100; b) H. Yan, H. S. Choe, S. W. Nam, Y. J. Hu, S. Das, J. F. Klemic, J. C. Ellenbogen, C. M. Lieber, *Nature* **2011**, *470*, 240.